Spatial distribution of information effective for logic function learning in spin-wave reservoir computing chip utilizing spatiotemporal physical dynamics

Takehiro Ichimura
Dept. of E.E. & Info. Sys.
The University of Tokyo
Tokyo, Japan
ichimura@eis.t.u-tokyo.ac.jp

Ryosho Nakane
Inst. for Innovation in IEE
The University of Tokyo
Tokyo, Japan
nakane@cryst.t.u-tokyo.ac.jp

Gouhei Tanaka
Inst. for Innovation in IEE
The University of Tokyo
Tokyo, Japan
gouhei@sat.t.u-tokyo.ac.jp

Akira Hirose
Dept. of E.E. & Info. Sys.
The University of Tokyo
Tokyo, Japan
ahirose@ee.t.u-tokyo.ac.jp

***Abstract*—This paper investigates the spatial distribution of information effective for function learning in a spin-wave reservoir-computing garnet chip. We map the neural weights of a readout neuron virtually connected massively and densely to the reservoir chip. We find that the spatial weight distribution shows wavefront-like lines, suggesting the importance of concurrent and time-different interferences of the spin waves. We also estimate the size of reservoir output electrodes required for the proper information extraction. These results are significantly useful for designing spin reservoir chips in the near future energy efficient devices.**

***Index Terms*—Neural hardware, physical reservoir computing, spin wave, energy-efficient neural chip**

I. Introduction

Reservoir computing dates back to the echo state network [1], [2] and the liquid state machine [3], [4]. It shows high ability to cope with difficult tasks when equipped with sufficient number of neurons with relatively small calculation costs even for time-sequential problems. Many researchers reported their analyses [5]–[7] including the utilization of the so-called edge of chaos [8], [9], performance analyses in terms of embedding dimension [10], nonlinearity in constructing elements such as memristor [11] and its variability among the elements [12].

One of the most important features in reservoir computing is the possibility that it is realizable directly based on physical phenomena, resulting in physical reservoir computing [13]. Various ideas have been presented such as the use of water in a bucket [14] and soft matter like silicon-rubber octopus feet [15], [16] as well as optics [17]–[19], optoelectronics [20] and electronics [21]. Other proposals use leading edge technologies such as spin torque [22], skyrmions [23], nano-magnetic dots [24] and spin waves [25], [26]. The good matching with physical phenomena leads to the realization of "devices with no need of elaboration" to open a new paradigm of information devices [27].

Reservoir is also highly compatible with wave and oscillation phenomena, resulting in proposals of coupled-oscillator based reservoir [28] and external-cavity laser based one [29]. In this aspect, reservoir has strong connections with various areas of wave-based neural processing architecture such as wave-based chip [30], carrier-wave computing [31] and complex-valued neural networks [32]. This feature enhances the connections to widely wave-based neural networks [33], [34] such as lightwave neural networks [35]–[38].

In these years, system constructions and demonstrations are also attracting many researchers, namely, distinction of sinusoidal and rectangular waves [39], voice classification [40], information traffic control in internet of things (IoT) networks [41], and some others.

In this paper, we focus on the spin-wave reservoir computing using garnet films [25]. Spin-wave dynamics is explained by the Landau-Lifshits motion equation. It has been revealed to present very small energy consumption in its propagation in comparison with other waves or currents, and suitable as the basis of energy-saving devices in the near future [42]. Spin-wave dynamics is very complicated due to its nonlinearity, spatial anisotropy, hysteresis and dispersion. Such complexity in the dynamics will realize ideal physical reservoir computing.

This paper analyzes where on the garnet film meaningful information localizes spatially two-dimensionally by physical numerical-calculation experiments. This analysis is a starting point of the construction of design-method framework of spin-wave-based reservoir chips and hardware.

II. Construction of the spin-wave reservoir

Fig. 1(a) shows the total construction of a reservoir computing neural system. Fig. 1(b) is a conceptual illustration showing the basic structure of the garnet-film spin reservoir. Physical details are given in literature [25], [26]. The dynamics is explained simply as follows. Voltage signals applied at input terminals trigger spin waves in the garnet film through the magneto-electric (ME) coupling. The spin waves propagate, interfere and bounce at the edges with nonlinearity, anisotropy and hysteresis. These phenomena transform the time-sequential input signals into complicated spatiotemporal

This work was supported in part by JSPS KAKENHI Grant No. 18H04105 (AH) and also by the New Energy and Industrial Technology Development Organization (NEDO) (AH, RN, GT).

978-1-7281-6926-2/20/$31.00 ©2020 IEEE

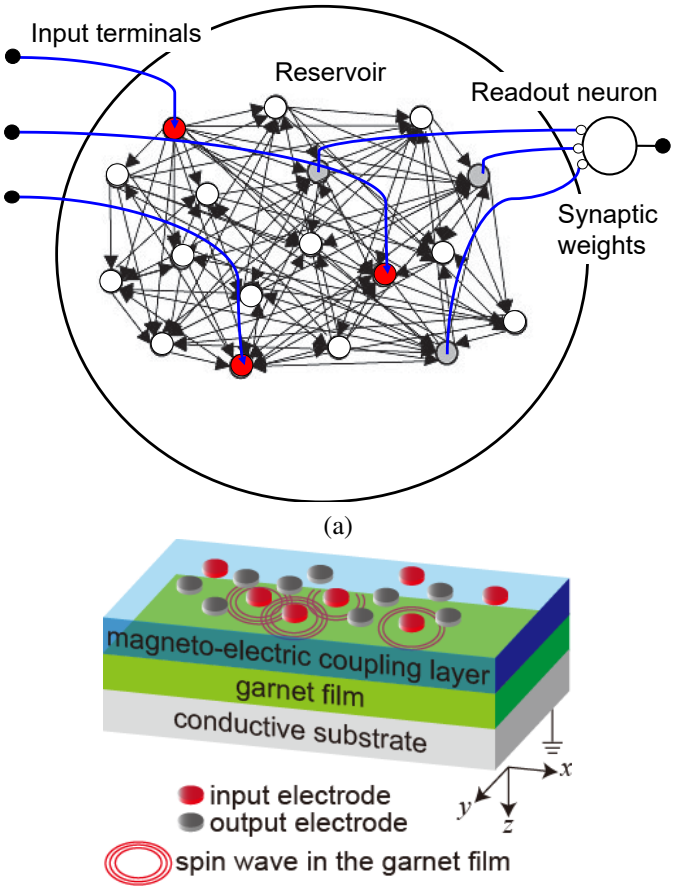

Fig. 1. (a) General construction of a reservoir computing system in total and (b) basic structure of the spin wave reservoir chip [25].

signals, which realize an effective reservoir. Note that, here in the film, there are almost infinite number of spins working as neurons, which is an ideal situation for reservoir computing. Then the output electrodes pick up the generated wave signals by the ME coupling.

The spin waveform in the garnet film depends on the input voltage signal. In most cases, when we apply square wave just like in the present case, we will observe clear spin-wave generation at the rising and falling edges, showing low frequency spin waves determined by the ferromagnetic resonance (FMR). In contrast, if we apply a signal higher than its FMR frequency continuously, then we will find a high frequency waveform following the input signal. In this paper, we employ square waveform inputs.

III. Physical Numerical-Calculation Experiments and Results

A. General setup and dynamics of reservoir and neuron

Fig. 2 shows the dimension of the film chip as well as the sizes and positions of the input electrodes A and B. We assume a task of time-sequential exclusive OR (time-sequential XOR) in this paper. XOR task is suitable for examining the basic properties of the reservoir dynamics since it is the simplest

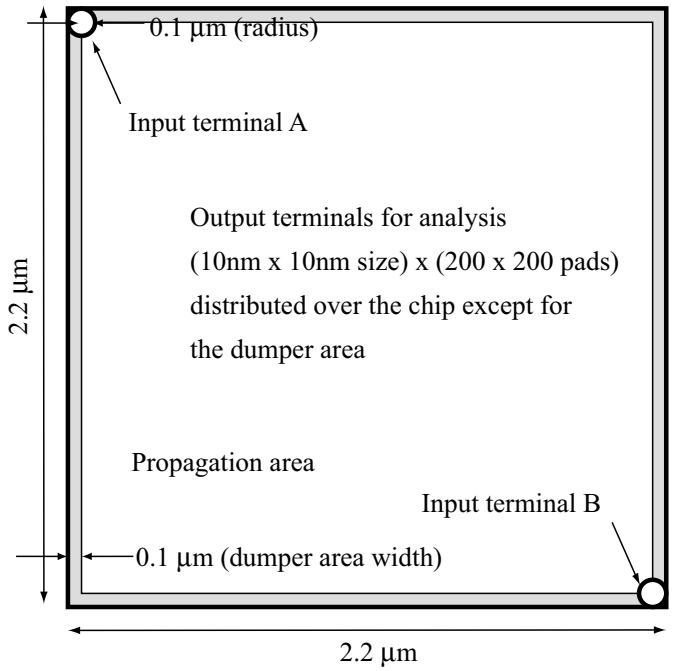

Fig. 2. Dimension of the garnet film with partially absorptive boundary and the positions of input terminals A and B.

linearly non-separable problem. For input terminals A and B, we prepare "0" "0", "0" "1", "1" "0" and "1" "1" time-sequential inputs as shown in Fig. 3, where the voltage waveforms similar to those in our previous work [25]. Time frame n corresponds to an n-th single symbol time.

The physical property to be modulated is the magnetocrystalline uniaxial anisotropy constant K_u in the film. In the following physical-numerical experiments, we used MuMax3 simulator [43]. The spatial mesh size is 1 μm square, and the time step is 0.01 ns.

We use the same parameters as those in literature [25], that is, the film thickness is 100 nm, the mesh size in z-direction 50 nm, the damping constant α = 0.001 (garnet film) or 1 (damper), the saturation magnetization M_S = 100 kA/m, the exchange stiffness constant $A_{\mathrm{EX}} = 3.6 \times 10^{-12}$ J/m, the z-direction uniaxial magnetic anisotropy constant for the max input voltage $K_{\mathrm{U}}^{\mathrm{L}}$ (1 kJ/m^3), that for zero input voltage $K_{\mathrm{U}}^{\mathrm{H}}$ (10 kJ/m^3) and the cubic magnetocrystalline anisotropy constant K_{C} = 0. These parameters are quite reasonable for common garnets such as $\mathrm{Tm_3Fe_5O_{12}}$ and $\mathrm{Y_3Fe_5O_{12}}$. The analysis temperature is 0 K only just for simplicity.

Fig. 4 shows the total construction of the reservoir neural network. The output of the reservoir is fed to a readout neuron. For the numerical analysis in this paper, we prepare about 220×220 very small and dense output electrodes virtually pixel by pixel of the numerical mesh size. The reservoir output $\boldsymbol{x}$ are simply preprocessed and fed to the readout neuron through weights $\boldsymbol{w}$. The neuron can be a linear weight-and-sum. But, in this numerical experiment, it is assumed to have an activation function $f(u) = (1/(1+\exp(-u)))$ to generate a neural output corresponding to the saturation nonlinearity in

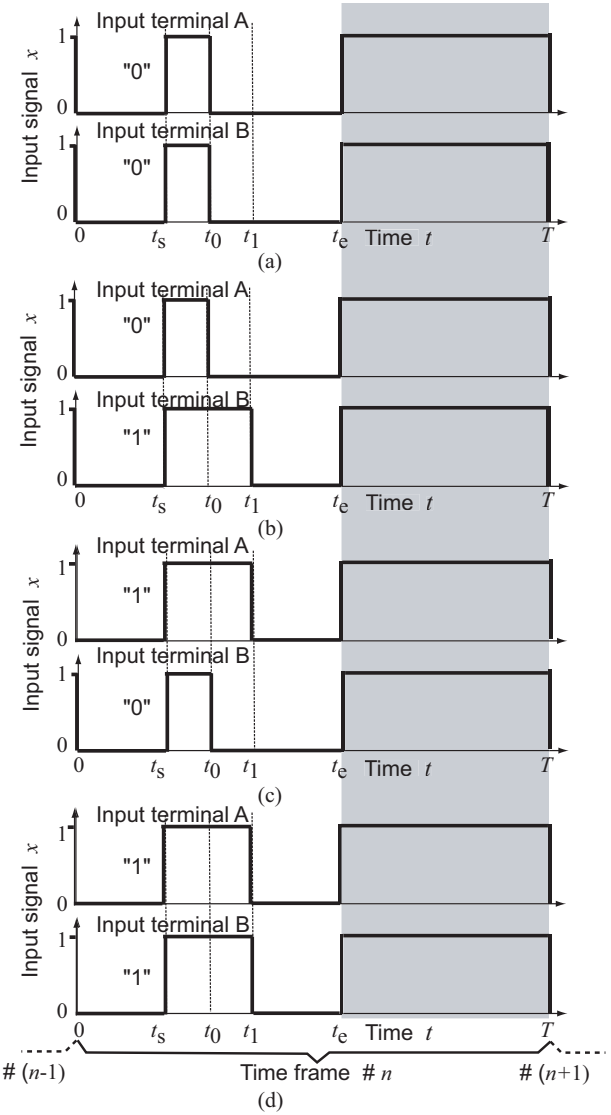

Fig. 3. Input teacher waveforms of (a) "0""0", (b) "0""1", (c) "1""0" and (d) "1""1" for the time-sequential XOR learning. The hatch shows the time region used for the learning and decision.

the electronics. The neuron has a bias term as well.

Note that the huge number of reservoir output electrodes are prepared just only for the present numerical analysis. In a practical case, we make much fewer, appropriately sized electrodes. For this purpose, it has critical importance to obtain physical and structural knowledge in the following experimental analysis.

In this experiment, we observe the amplitude at position $\boldsymbol{r}$ averaged over the time period from $t = t_{\rm e}$ to T (hatched in Fig. 3) with a rectification and low-pass filtering (LPF) preprocessing. That is,

$$\overline{\boldsymbol{x}}(\boldsymbol{r}, n) = \frac{1}{T - t_{\rm e}} \int_{t_{\rm e}({\rm frame}\ n)}^{T} {\rm Amp}\left(\boldsymbol{x}(t, \boldsymbol{r})\right) dt \quad (1)$$

$$y(n) = f\left(\boldsymbol{w}(\boldsymbol{r}) \cdot \overline{\boldsymbol{x}}(\boldsymbol{r}, n)\right) \quad (2)$$

where ${\rm Amp}(\cdot)$ denotes amplitude extraction. This process is

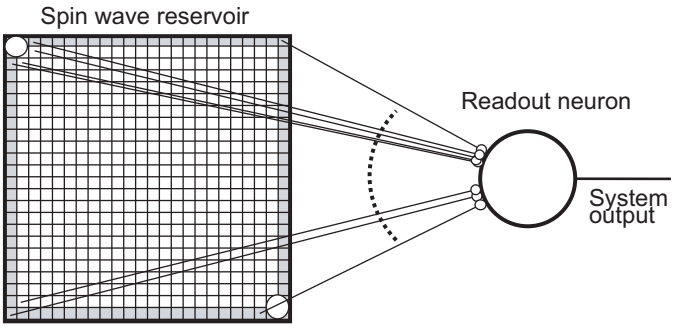

Fig. 4. System construction showing the connections between spin reservoir output terminals and a readout neuron.

realized by a diode and a LPF very easily in reality. A neuron bias w_0 is also included in $\boldsymbol{w}$ by assuming $x_0 = -1$. In (2), n is an index for time frame as we explained in Fig. 3. In the present task, every time-sequential signal is processed within a single time frame almost independently though there exists time-dependent processing within a time frame. We apply a supervised learning employing the gradient descent method to minimize the difference of neural output $y(n)$ and the XOR teacher signal $\hat{y}(n)$=1 or 0 with a mini batch process to realize online adaptability.

We divide a total set of N data into $N/N_{\rm mini}$ subsets, each of which consists of $N_{\rm mini}$ data corresponding to a mini batch. A set of mini batch data updates the weights $\boldsymbol{w}$ to a new $\boldsymbol{w}_{\rm new}$ as

$$\boldsymbol{w}(\boldsymbol{r})_{\rm new} = \boldsymbol{w}(\boldsymbol{r}) + \Delta\boldsymbol{w}(\boldsymbol{r}) \quad (3)$$

$$\Delta\boldsymbol{w}(\boldsymbol{r}) = -\frac{\eta}{N_{\rm mini}} \sum_{n=0}^{N_{\rm mini}} (y(n) - \hat{y}(n)) f'(\boldsymbol{w}(\boldsymbol{r}) \cdot \overline{\boldsymbol{x}}) \overline{\boldsymbol{x}}(\boldsymbol{r}) \quad (4)$$

where η is a learning rate, $y(n)$ is the neural output at time frame n, and $\hat{y}(n)$ is the teach signal. We iterate or continue this update so that the neural system follows even a changing environment. We call the single learning with all mini-batch datasets one epoch. We set the time parameters in Fig. 3 as, $t_{\rm s}$=3 ns, t_0=4.5 ns, t_1=6 ns, $t_{\rm e}$=9 ns and T=16 ns.

B. Results of physical numerical-calculation experiments

Fig. 5 shows the spin waveforms of (a) x- and (b) y-direction spin components, s_x and s_y observed at the center of the garnet film when input signals of A: "0" and B: "1" are fed. Spin waves are observed after the input triggers ($t = 0$) with small time delays. Though the input signals are simple, the observed waves are very complicated.

Fig. 6 shows the time evolution of the spatial weight distribution $\boldsymbol{w}(\boldsymbol{r})$ according with the iteration of the learning epoch. The weights are initialized at random (Fig. 6(a)). Through the learning process, a spatial structure gradually appears. The areas showing strong intensities (positive: red areas, negative: blue areas) look like wave fronts. The positive and negative areas are distributed separately at the central

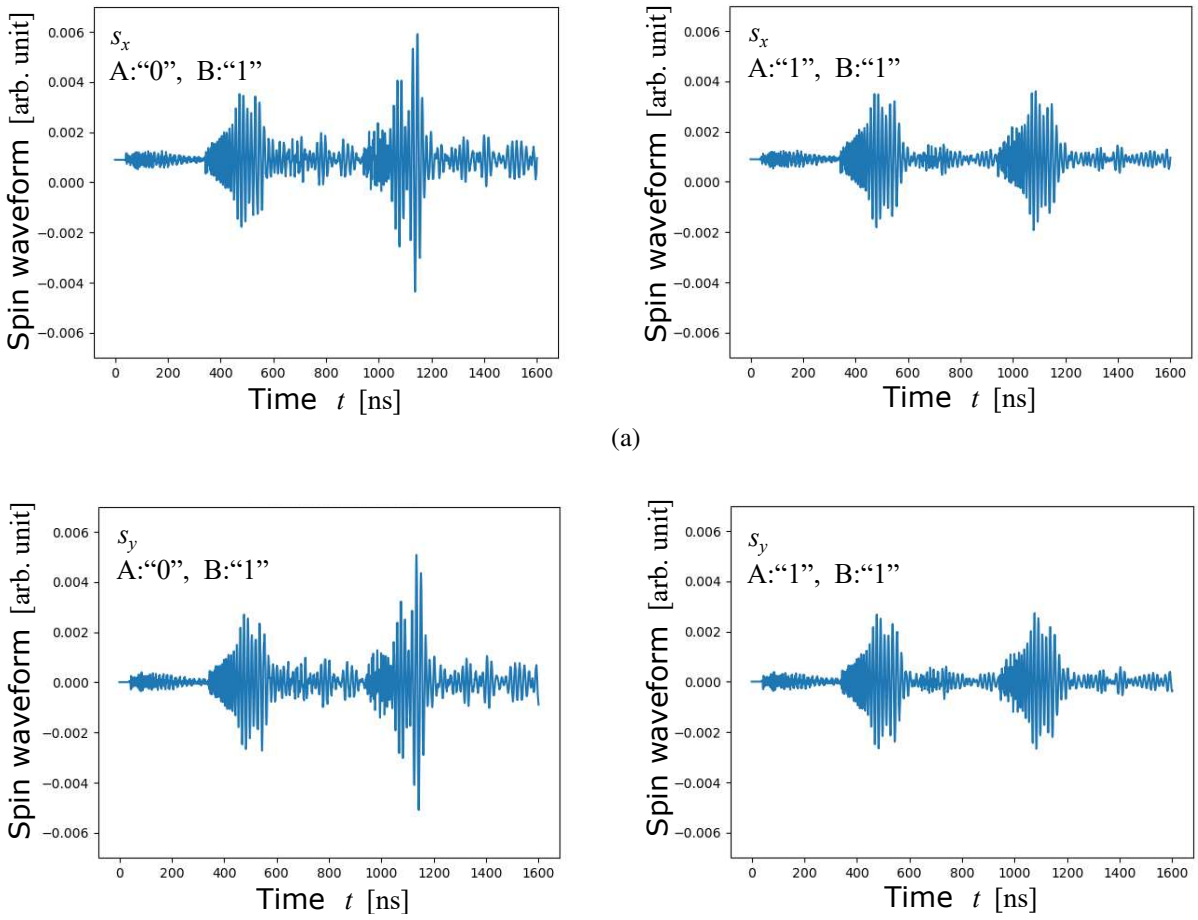

Fig. 5. Waveforms of (a) x- and (b) y-direction spin components, s_x and s_y, at the center of the film for input signals of (left) A:”0”and B:”1” and (right) A:”1”and B: ”1”, respectively.

coincidently interfering part and at the non-central time-differently interfering parts.

Fig. 7 is the learning curve. It shows a smooth convergence. Fig. 8 presents the neuron output for the four pairs of input signals (a) before and (b) after the learning. Before the learning, the output is medium for all the input pairs. However, after the learning, we find the output presents the XOR logic successfully. Since the number of neurons are almost infinitely large, there is very small variability in the output levels in both the before and after learning outputs.

Fig. 9 shows the reservoir outputs in time average (t = 9 to 16 ns) for input signals of (a) “0”“0”, (b) “0”“1”, (c) “1”“0”, (d) “1”“1”, respectively. They are somewhat similar, but actually different. The readout neuron learned to detect the difference.

For comparison, Fig. 10 shows the map of the effective reservoir output, that is, the rectified and low-pass-filtered reservoir outputs, time-averaged in t=9 – 16 ns, for inputs “A:0” B:“0” and A:“1” B:“1” but subtracted by those for inputsA:“1” B:“0” and A:“0” B:“1”, that is, $\{$(a)+(d)$\}-\{$(b)+(c)$\}$ in Fig. 9. This should be the effective XOR information distributed on the garnet film. This distribution is very similar to the convergence result in Fig. 6, which means that the neuron learned the time-sequential XOR feature properly as we expect. Note that the learning in reservoir computing deals with time-sequential signals. Within each time frame, the learning process utilizes the time-sequential feature. This fact results in the difference in the weight distribution showing the concurrent and time-different interferences.

The high similarity between the weight distribution in Fig. 6 and the effective signal distribution in Fig. 10 represents the fact that the reservoir neural network extracted useful features successfully in the learning. We have confirmed that the spin-wave reservoir provides the readout neuron with useful information by utilizing the physical dynamics spatiotemporally.

In addition, we find that the reservoir output electrodes can be several tens nm in its diameter to extract the features. This is shown in the spatial distribution of the weights having about several tens nm or larger spatial variations. We can also find in the rough positive/negative distribution that several or a few

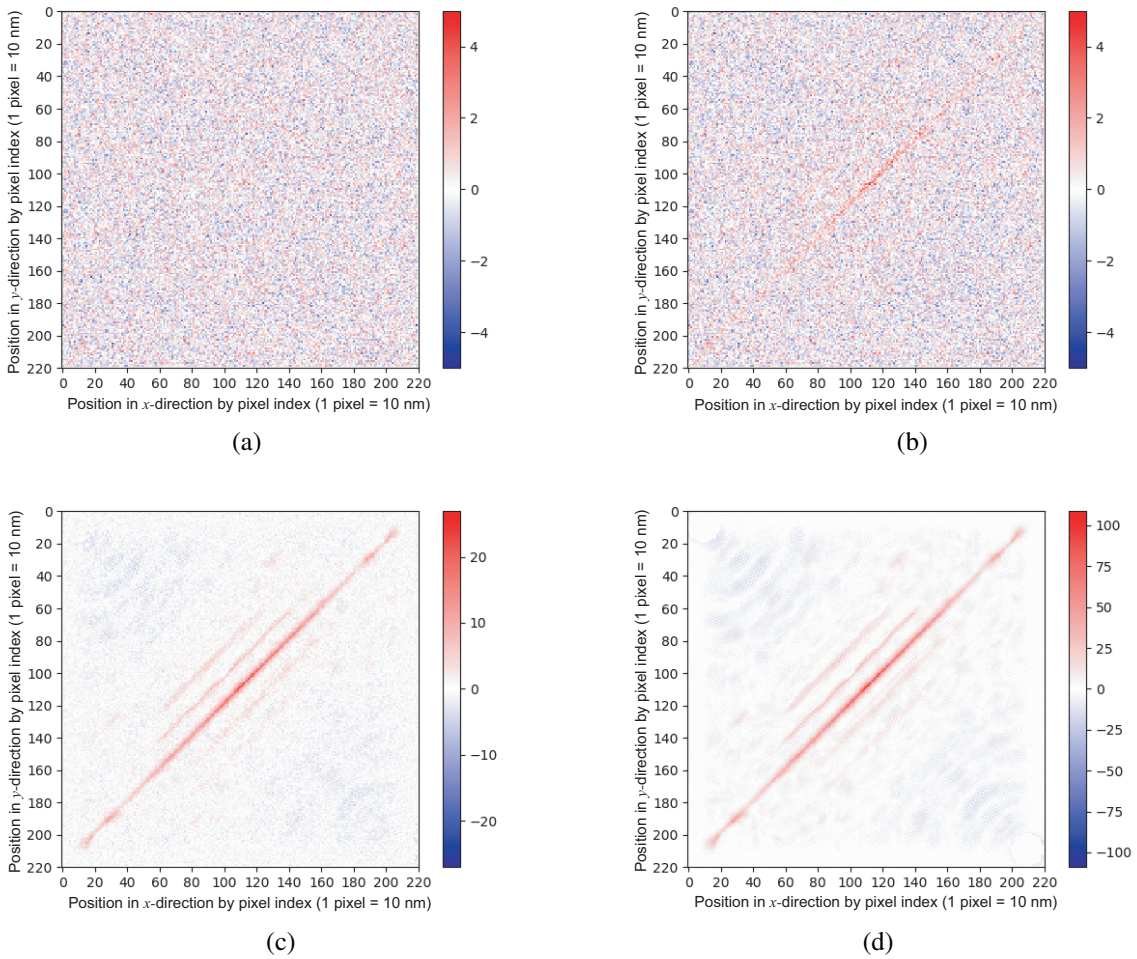

Fig. 6. Neural weight distribution when the learning iteration is (a) 1,000 epochs, (b) 10,000 epochs, (c) 100,000 epochs and (d) 1,000,000 epochs, respectively.

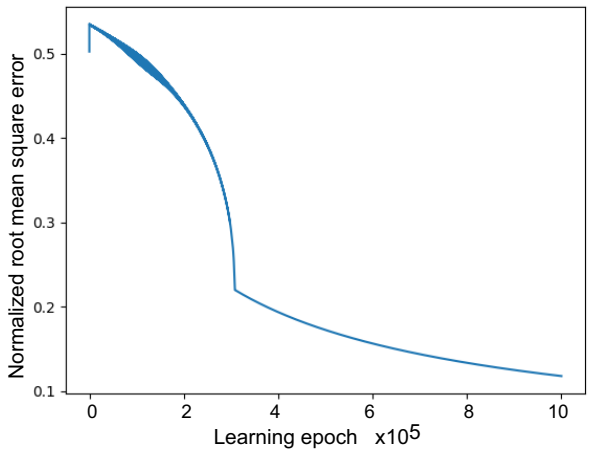

Fig. 7. Learning curve showing the root mean square error versus learning epochs.

tens electrodes will be sufficient for picking up the features well in the present task.

IV. Conclusion

This paper demonstrated that the spin-wave reservoir computing solves the problem by utilizing its spatiotemporal physical dynamics. In particular, we observed the spatial distribution of information effective for time-sequential XOR logic learning. We found that the weight distribution is very similar to that of the signal difference between same-input and different-input reservoir responses, which means that the neuron learned the XOR feature properly. The information effective for the function learning presents a wavefront-like pattern indicating to concurrent and time-different interference. We also found that the reservoir output electrodes can be several tens nm in its diameter to extract the features. These results have high significance in designing a spin-wave reservoir computing chip for various adaptive information processing.

References

[1] H. Jaeger, “The ”echo state” approach to analysing and training recurrent neural newtorks – With an erratum note,” German National Research

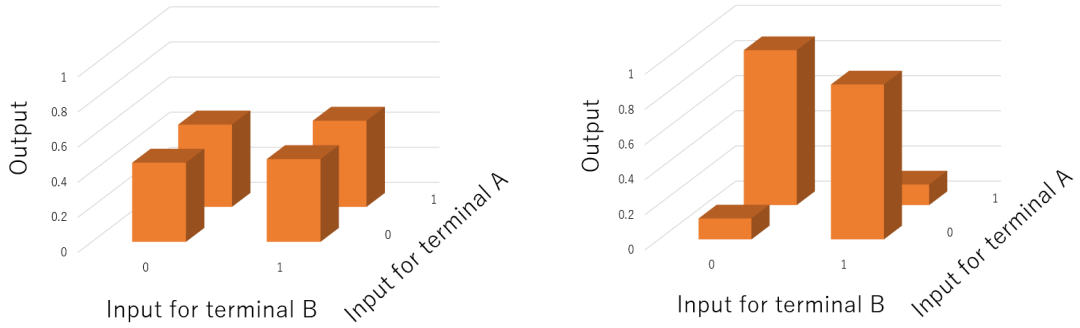

Fig. 8. Neuron output for the four pairs of input signals representing time-sequential XOR (a) before and (b) after the learning.

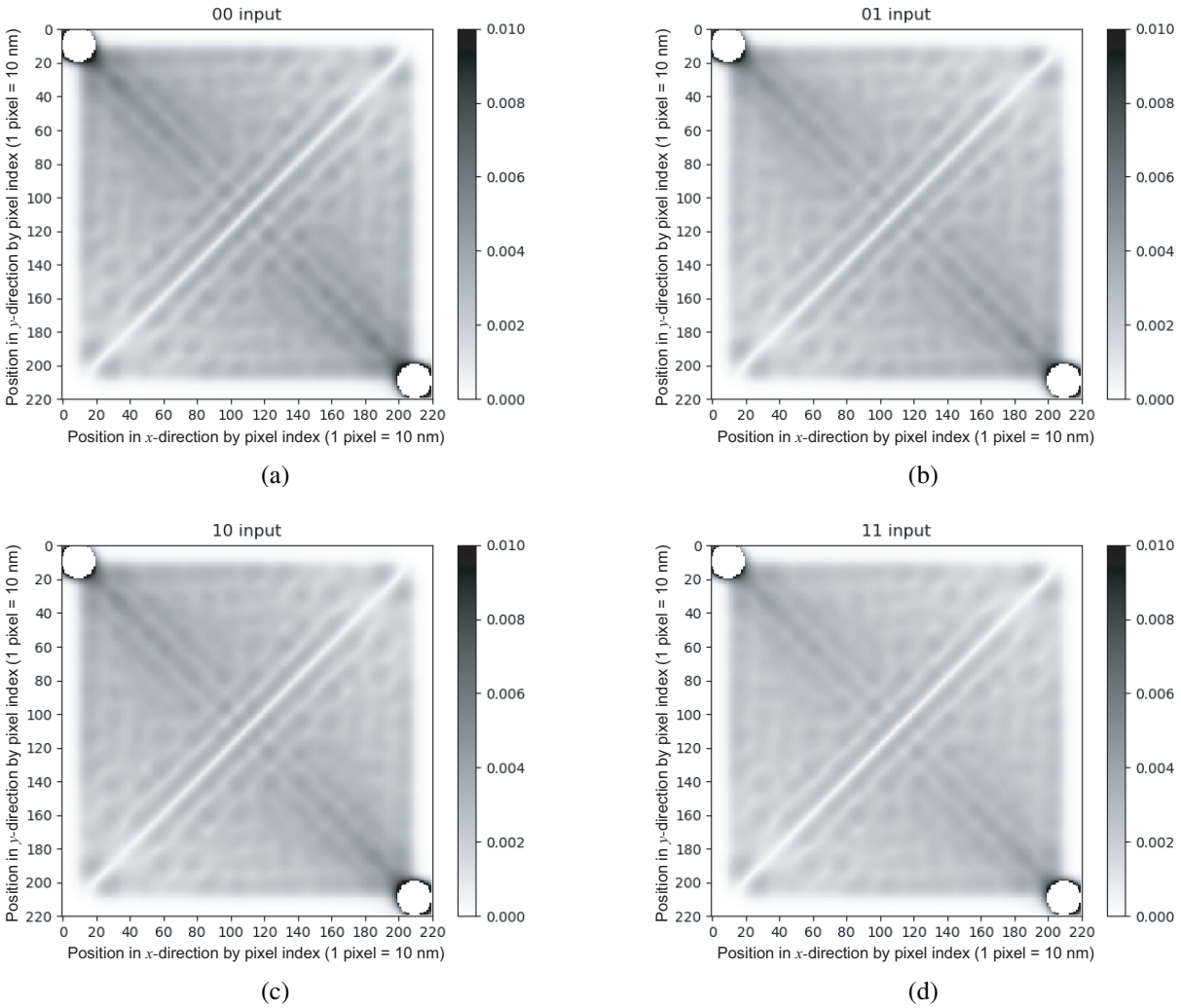

Fig. 9. Distribution of time-averaged reservoir outputs at respective mesh for input signals of (a) ”0” ”0”, (b) ”0” ”1”, (c) ”1” ”0” and (d) ”1” ”1”, respectively.

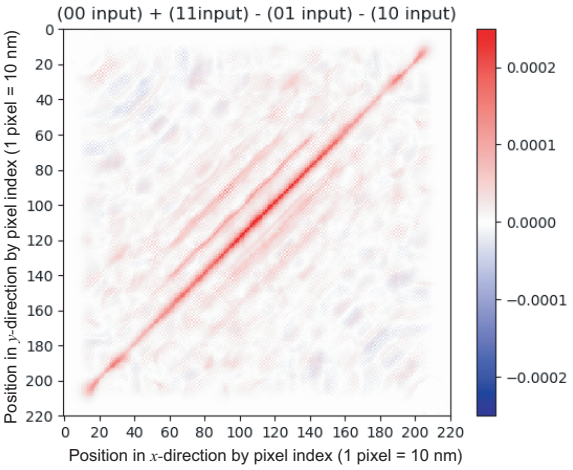

Fig. 10. Distribution of the reservoir output difference calculated as ((a)+(d))−((b)+(c)) in Fig. 9, which is expected to be effective for the time-sequential XOR learning.

Center for Information Technology (GMD), Bonn, Germany, Technical Report 148, 13, 2001.

[2] H. Jaeger and H. Haars, "Harnessing nonlinearity: Predicting chaotic systems and saving energy in wireless communication," *Science*, vol. 304, pp. 78–80, April 2004.

[3] W. Maass, T. Natschlänger, and H. Markram, "Real-time computing without stable states: A new framework for neural computation based on perturbations," *Neural Computation*, vol. 14, no. 11, pp. 2531–2560, 2002.

[4] W. Maass, *Computability in Context*. World Scientific, 2011, ch. Liquid state machines : Motivation, theory, and applications, pp. 275–296.

[5] D. Verstraeten, B. Schrauwen, M. D'Haene, and D. Stroobandt, "An experimental unification of reservoir computing methods," *Neural Networks*, vol. 20, no. 3, pp. 391–403, April 2007.

[6] M. Lukosevicius and H. Jaeger, "Reservoir computing approaches to recurrent neural network training," *Computer Science Review*, vol. 3, no. 3, pp. 127–149, August 2009.

[7] R. Mori, G. Tanaka, R. Nakane, A. Hirose, and K. Aihara, "Computational performance of echo state networks with dynamic synapses," in *International Conference on Neural Information Processing (ICONIP) 2016 Kyoto*, 2016, pp. 264–271.

[8] N. Bertschinger and T. Natschlger, "Real-time computation at the edge of chaos in recurrent neural networks," *Neural Computation*, vol. 16, no. 7, pp. 1413–1436, 2004. [Online]. Available: https://doi.org/10.1162/089976604323057443

[9] T. Yamane, S. Takeda, D. Nakano, G. Tanaka, R. Nakane, S. Nakagawa, and A. Hirose, "Dynamics of reservoir computing at the edge of stability," in *International Conference on Neural Information Processing (ICONIP) 2016 Kyoto*, 2016, pp. 205–212.

[10] T. Yamane, S. Takeda, D. Nakano, G. Tanaka, R. Nakane, A. Hirose, and S. Nakagawa, "Simulation study of physical reservoir computing by nonlinear deterministic time series analysis," in *International Conference on Neural Information Processing (ICONIP) 2017 Guangzhou*, 2017, pp. 639–647.

[11] G. Tanaka, R. Nakane, T. Yamane, S. Takeda, D. Nakano, S. Nakagawa, and A. Hirose, "Nonlinear dynamiccomdynamic of memristive networks and its application to reservoir computing," in *International Symposium on Nonlinear Theory and Its Applications (NOLTA) 2017 Cancun*, A2L-E-2, 2017.

[12] G. Tanaka, R. Nakane, T. Yamane, D. Nakano, S. Takeda, S. Nakagawa, and A. Hirose, "Exploiting heterogeneous units for reservoir computing with simple architecture," in *International Conference on Neural Information Processing (ICONIP) 2016 Kyoto*, 2016, pp. 187–194.

[13] G. Tanaka, T. Yamane, J. B. Héroux, R. Nakane, N. Kanazawa, S. Takeda, H. Numata, D. Nakano, and A. Hirose, "Recent advances in physical reservoir computing: A review," *Neural Networks*, vol. 115, pp. 100–123, 2019.

[14] C. Fernando and S. Sojakka, "Pattern recognition in a bucket," in *Advances in Artificial Life*, 2003, pp. 588–597.

[15] K. Nakajima, H. Hauser, T. Li, and R. Pfeifer, "Information processing via physical soft body," *Scientific reports*, vol. 5, p. 10487, 2015.

[16] K. Nakajima, T. Li, H. Hauser, and R. Pfeifer, "Exploiting short-term memory in soft body dynamics as a computational resource," *Journal of The Royal Society Interface*, vol. 11, p. 20140437, June 2018.

[17] Y. Paquot, F. Duport, A. Smerieri, J. Dambre, B. Schrauwen, M. Haelterman, and S. Massar, "Optoelectronic reservoir computing," *Scientific reports*, vol. 2, p. 287, 2012.

[18] L. Larger, M. C. Soriano, D. Brunner, L. Appeltant, J. M. Gutierrez, L. Pesquera, C. R. Mirasso, and I. Fischer, "Photonic information processing beyond turing: an optoelectronic implementation of reservoir computing," *Optics Express*, vol. 20, no. 3, pp. 3241–3249, 2012.

[19] J. Bueno, S. Maktoobi, L. Froehly, I. Fischer, M. Jacquot, L. Larger, and D. Brunner, "Reinforcement learning in a large-scale photonic recurrent neural network," *Optica*, vol. 5, no. 6, pp. 756–760, Jun 2018. [Online]. Available: http://www.osapublishing.org/optica/abstract.cfm?URI=optica-5-6-756

[20] P. Antonik, F. Duport, A. Smerieri, M. Hermans, M. Haelterman, and S. Massar, "Online training of an opto-electronic reservoir computer," in *International Conference on Neural Information Processing (ICONIP) 2015 Istanbul*, vol. 2, 2015, pp. 233–240.

[21] Y. Yi, Y. Liao, B. Wang, X. Fu, F. Shen, H. Hou, and L. Liu, "FPGA based spike-time dependent encoder and reservoir design in neuromorphic computing processors," *Microprocessors and Microsystems*, vol. 46, pp. 175 – 183, 2016. [Online]. Available: http://www.sciencedirect.com/science/article/pii/S0141933116300060

[22] S. Tsunegi, T. Taniguchi, K. Nakajima, S. Miwa, K. Yakushiji, A. Fukushima, S. Yuasa, and H. Kubota, "Physical reservoir computing based on spin torque oscillator with forced synchronization," *Appl. Phys. Lett.*, vol. 114, no. 16, p. 164101, Jan. 2020. [Online]. Available: https://doi.org/10.1063/1.5081797

[23] D. Prychynenko, M. Sitte, K. Litzius, B. Krüger, G. Bourianoff, M. Kläui, J. Sinova, and K. Everschor-Sitte, "Magnetic skyrmion as a nonlinear resistive element: A potential building block for reservoir computing," *Phys. Rev. Applied*, vol. 9, p. 014034, Jan 2018. [Online]. Available: https://link.aps.org/doi/10.1103/PhysRevApplied.9.014034

[24] H. Nomura, T. Furuta, K. Tsujimoto, Y. Kuwabiraki, F. Peper, E. Tamura, S. Miwa, M. Goto, R. Nakatani, and Y. Suzuki, "Reservoir computing with dipole-coupled nanomagnets," *Japanese Journal of Applied Physics*, vol. 58, no. 7, p. 070901, jun 2019.

[25] R. Nakane, G. Tanaka, and A. Hirose, "Reservoir computing with spin waves excited in a garnet film," *IEEE Access*, vol. 6, pp. 4462 – 4469, 2018.

[26] ——, "Demonstration of spin-wave-based reservoir computing for next-generation machine-learning devices," in *International Conference on Magnetism (ICM) 2018 San Francisco*, July 2018, pp. 26–27.

[27] A. Hirose, S. Takeda, D. Nakano, T. Yamane, S. Nakagawa, R. Nakane, and G. Tanaka, "Complex-valued neural networks for wave-based realization of reservoir computing," in *International Conference on Neural Information Processing (ICONIP) 2017 Guangzhou*, 2017, pp. 449–456.

[28] T. Yamane, Y. Katayama, R. Nakane, G. Tanaka, and D. Nakano, "Wave-based reservoir computing by synchronization of coupled oscillators," in *International Conference on Neural Information Processing (ICONIP) 2015 Istanbul*, vol. 3, 2015, pp. 198–205.

[29] S. Takeda, D. Nakano, T. Yamane, G. Tanaka, R. Nakane, A. Hirose, and S. Nakagawa, "Photonic reservoir computing based on laser dynamics with external feedback," in *International Conference on Neural Information Processing (ICONIP) 2016 Kyoto*, 2016, pp. 222–230.

[30] Y. Katayama, T. Yamane, D. Nakano, R. Nakane, and G. Tanaka, "Wave-based neuromorphic computing framework for brain-like energy efficiency and integration," *IEEE Transactions on Nanotechnology*, vol. 15, no. 5, pp. 762–769, September 2016.

[31] A. Hirose, G. Tanaka, S. Takeda, T. Yamane, H. Numata, N. Kanazawa, J. B. Héroux, D. Nakano, and R. Nakane, "Proposal of carrier-wave reservoir computing," in *International Conference on Neural Information Processing (ICONIP) 2018 Siem Reap*, December 2018, pp. 616–624.

[32] A. Hirose, S. Takeda, D. Nakano, T. Yamane, S. Nakagawa, R. Nakane, and G. Tanaka, "Complex-valued neural networks to realize energy-efficient neural networks including reservoir computing," in *Interna-*

tional Symposium on Nonlinear Theory and Its Applications (NOLTA) 2017 Cancun, 2017, pp. 186–188.

[33] A. Hirose and R. Eckmiller, "Behavior control of coherent-type neural networks by carrier-frequency modulation," *IEEE Transactions on Neural Networks*, vol. 7, no. 4, pp. 1032–1034, 1996.

[34] ——, "Coherent optical neural networks that have optical-frequency-controlled behavior and generalization ability in the frequency domain," *Applied Optics*, vol. 35, no. 5, pp. 836–843, 1996.

[35] S. Kawata and A. Hirose, "Frequency-multiplexed logic circuit based on a coherent optical neural network," *Applied Optics*, vol. 44, no. 19, pp. 4053–4059, 2005.

[36] A. Limmanee, S. Kawata, and A. Hirose, "Phase signal embedment in densely frequency-multiplexed coherent neural networks," in *OSA Topical Meeting on Information Photonics (OSA–IP) 2005 Charlotte*, no. ITuA2, June 2005.

[37] S. Kawata and A. Hirose, "Coherent optical neural network that learns desirable phase values in frequency domain by using multiple optical-path differences," *Optics Letters*, vol. 28, no. 24, pp. 2524–2526, 2003.

[38] ——, "Frequency-multiplexing ability of complex-valued Hebbian learning in logic gates," *International Journal of Neural Systems*, vol. 12, no. 1, pp. 43–51, 2008.

[39] G. Tanaka, R. Nakane, T. Yamane, S. Takeda, D. Nakano, S. Nakagawa, and A. Hirose, "Waveform classification by memristive reservoir computing," in *International Conference on Neural Information Processing (ICONIP) 2017 Guangzhou*, 2017, pp. 457–465.

[40] J. Torrejon, M. Riou, F. A. Araujo, S. Tsunegi, G. Khalsa, D. Querlioz, P. Bortolotti, V. Cros, K. Yakushiji, A. Fukushima, H. Kubota, S. Yuasa, M. D. Stiles, and J. Grollier, "Neuromorphic computing with nanoscale spintronic oscillators," *Nature*, vol. 547, pp. 428–431, July 2017.

[41] T. Yamane, H. Numata, J. B. Héroux, N. Kanazawa, S. Takeda, G. Tanaka, R. Nakane, A. Hirose, and D. Nakano, "Dimensionality reduction by reservoir computing and its application to iot edge computing," in *International Conference on Neural Information Processing (ICONIP) 2018 Siem Reap*, December 2018, pp. 635–644.

[42] N. Kanazawa, T. Goto, K. Sekiguchi, A. B. Granovsky, C. A. Ross, H. Takagi, Y. Nakamura, and M. Inoue, "Demonstration of a robust magnonic spin wave interferometer," *Scientific Reports*, vol. 6, no. 1, p. 30268, Jul. 2016. [Online]. Available: https://doi.org/10.1038/srep30268

[43] A. Vansteenkiste, J. Leliaert, M. Dvornik, M. Helsen, F. Gracia-Sanchez, and B. Van Waeyenberge, "The design and verification of MuMax3," *AIP Advances*, vol. 4, no. 10, October 2014.